Desalination mechanism of modified activated carbon/carbon nanotubes composite electrode

Wang Li, Hu Yusha, Lu Yifei, Fu Jiangtao, Hu Ning and Ma Li

ABSTRACT

Modified activated carbon/carbon nanotubes (AC*/CNT*) composite electrode was used as the electrode in a capacitive deionization (CDI) process for desalination in this study. The morphology and electrochemical characteristics of the modified electrode were discussed, and the results showed that after modification, the specific surface area of AC* reached 672.48 m^2/g, increased by 29.43%; while the specific surface area of CNT* was 117.39 m^2/g, reduced by 9.94% due to the strong oxidation of the mixed acid, the pore volume of CNT* increased by 48.28%. The electrode regeneration test proved that the electrode had good cycling stability. The pseudo-first-order kinetic model could better describe the adsorption rate of the electrodes for ions and the desalination ratio of the AC*/CNT* electrode reached 7.11 mg/g; the Langmuir model could well describe the adsorption mechanism of capacitive deionization, and indicated that the adsorption process of CDI was near to single ion layer adsorption; the change trend of electric mobility with migration time could be well fitted by exponential equations. This study explored a novel composite electrode coating, and initially explored the behavioral characteristics and trends of CDI technology.

Key words | activated carbon, capacitive deionization (CDI), carbon nanotube, mechanism analysis, modification

Wang Li (corresponding author)
Hu Yusha
Lu Yifei
Fu Jiangtao
Hu Ning
College of Natural Resources and Environmental Protection,
Wuhan University of Science and Technology,
Wuhan, 430081,
China
E-mail: *wanglijohn@163.com*

Ma Li
Wuhan Safety and Environmental Protection Research Institute,
Wuhan, 430081,
China

INTRODUCTION

Capacitive deionization technology, as a new water treatment technology based on double layer capacitance theory (Wang *et al.* 2015; Kang *et al.* 2016), has a crowd of characteristics, such as high water yield, low energy consumption, environmental friendliness, simple equipment, easy operation and so on (Hou *et al.* 2013; Porada *et al.* 2013). There are broad prospects for the desalting of high salty mining waste water (Huang *et al.* 2014), the deep purification of drinking water (Orha *et al.* 2017), the softening of industrial water (Mossad & Zou 2012), and the removal of heavy metals from wastewater (Iftekhar *et al.* 2016). At present, most of the studies at home and abroad are focused on the selection and processing of capacitive deionized electrode materials and process parameters, and CDI efficiency is largely dependent on the specific surface area and electronic conductivity of the electrode materials (Santoro *et al.* 2017). Carbon materials, such as active carbon (Fang *et al.* 2016; Liu *et al.* 2016; Jo *et al.* 2017), activated carbon fiber (Wu *et al.* 2015; Bian *et al.* 2016), carbon aerogel (Kohli *et al.* 2012; Kumar *et al.* 2016), carbon nanotube (Hou *et al.* 2014; Li *et al.* 2016; Wang *et al.* 2017), graphene (Tuan *et al.* 2015; Xu *et al.* 2015; Dursun *et al.* 2017) and other single porous carbon materials have been studied in the field of polarizing electrode adsorption materials due to their high surface and good electronic conductivity, but there are few studies on composite electrodes modified by carbon electrodes. Activated carbon (AC) has been used as the electrode material mostly because of its large specific surface area, however, the amount of electrode adsorption will be seriously affected by its characteristics of poor conductivity and slow charge

doi: 10.2166/ws.2019.082

transfer, therefore, an effective way of enhancing the performance of the electrode is by improving the conductivity of the activated carbon electrode. Carbon nanotubes (CNTs) are considered to be an ideal CDI electrode conductive agent owing to their large specific surface area, good electrical conductivity, high stability, and the ability to form an electrically conductive network with large length-to-diameter ratios.

Therefore, CNTs were used as the conductive agent to prepare the AC*/CNT* composite electrode in this experiment; morphological characteristics and electrode regeneration performance were studied; in addition, the adsorption kinetics, adsorption isotherm and electromigration of the CDI desalination process were analyzed to fully understand the reaction process and mechanism of CDI.

METHODS

Electrode fabrication

(1) Activated carbon modification: Activated carbon (Zhongshan Activated Carbon Manufacturing Co. Ltd, Chongqing) was sieved by a 300 mesh sieve to remove large particles, then the activated carbon after screening was placed in HNO_3 solution, with ultrasound for 2 hours and then allowed to stand for 22 hours; after that, it was washed by deionized water to neutral, boiled for 2.5 hours and then washed until the conductivity was less than 10 μS/cm; finally, it was kept in vacuum drying at 75 °C for 12 hours.

(2) Carbon nanotube modification: After the condensate return and absorption device was installed, carbon nanotubes (Chengdu Organic Chemistry Co. Ltd, Chinese Academy of Sciences) were weighed in a three-neck flask, mixed acid (concentrated H_2SO_4 and concentrated HNO_3 according to the volume ratio of 3:1) was configured and added to the flask, and they were heated for 30 minutes in a 105 °C oil bath, then cooled to room temperature quickly, and washed to neutral with deionized water; after that, ultrasonic dispersion was used for 2 hours so that debris in the carbon nanotubes could be removed. They were soaked in deionized water and boiled for 3 hours, and washed to a conductivity of less than 10 μS/cm; finally, they were placed in a vacuum drying oven and dried at 75 °C for 12 hours.

(3) Preparation of electrodes: The prepared AC* and CNT* powders were made into a mixture according to different mass ratios and put into an electric drying oven and kept at 80 °C to dry; 2 g of polyvinylidene fluoride (PVDF, Arkema Chemical Co. Ltd) and 10 mL of dimethyl acetamide (DMAC) were weighed in a beaker and heated in a water bath at 80 °C until the PVDF was dissolved completely; then 8 g of the homogeneous mixture of AC* and CNT* at 80 °C was added to the beaker, and after stirring with a glass rod, 13 mL of N,N-dimethylacetamide (DMAC, H_2SO_4, HNO_3. Sinopharm Group Chemical Reagent Co. Ltd) was added to the beaker, heated and stirred sequentially, the precursor was obtained and spread on both surfaces of a titanium plate (50 mm × 50 mm × 1 mm, Northwest Institute of Nonferrous Metals) at 80 °C by a film applicator; and finally, electric heating at 85 °C was performed for 6 h to obtain an AC*/CNT* composite electrode, with 0.25 g of the mass of the active ingredient (AC* and CNT*) and 0.06 g of the mass of the binder (PVDF) in the two-surface coating of a single electrode.

Characterization experiments

The specific surface area and pore size distribution of AC, AC*, CNTs and CNT* were measured by surface area and pore size distribution analyzer (ASAP2020HD88, Micromeritics Instrument Corporation, USA). The cyclic voltammetry and electrochemical impedance spectroscopy measurements of the AC*/CNT* composite electrode were obtained by CHI660E electrochemical workstation (Shanghai CH Instruments Co. Ltd, Shanghai, China). The morphological characteristics of the CNT surface were observed by transmission electron microscope (JEM200CX, Japan Electronics Corporation, Japan). For an ideal cyclic voltammogram, the specific capacitance of the electrode is:

$$C = \frac{\int_{u_l}^{u_h} I(u)du}{2mv(u_h - u_l)} \quad (1)$$

where C is the mass ratio of the electrode material, F/g; m is the active ingredient mass, g; v is the scanning rate, V/s; I is

the current intensity, A; u_h and u_l are the highest and lowest voltage in the scanning process respectively, V.

Desalination experiments

The CDI system operated by this test was mainly composed of a DC stabilized power supply, a CDI module (containing two identically coated electrodes and a reaction chamber), a flow-controllable micro-pump, a digital display conductivity meter (ST3 100C, Ohaus Instruments Co. Ltd, Shanghai, China), and a beaker. Simulated salt water was 100 mg/L sodium chloride solution with a conductivity of 220 μS/cm at 25 °C, the initial influent concentration was 100 mg/L with a flow rate of 5 mL/min, the space between electrodes was 3 mm, and the working voltage was 1.2 V. The conductivity of the solution was measured at regular intervals by a conductivity meter.

RESULTS AND DISCUSSION

Performance analysis of activated carbon/carbon nanotube composite electrode

Specific surface area and pore size analysis of coating materials

The characterization of CNTs and CNT* is shown in Figure S1(a) and S1(b) (Supporting Information, available with the online version of this paper). Figure S1(a) shows that many black spots appeared in the CNT powder, which was formed by the aggregation of various carbon particle impurities, and the accumulation of entanglements between the carbon nanotube particles. Figure S1(b) shows that there were no black spots in the CNT* powder and each carbon nanotube particle existed independently. It shows that after strong acid oxidation, all impurities can be removed and purified, and the tube body of the carbon nanotubes can be 'cut' to increase the specific surface area effectively and improve the dispersibility.

The aperture distributions of AC, AC*, CNTs and CNT* based on the Barrett-Joyner-Halenda (BJH) method are shown in Figure S1(c); the pore volumes of AC* and CNT* were significantly larger than the pore volumes before modification. The microstructure parameters of AC, CNTs, AC* and CNT* are listed in Table S1 (Supporting Information, available online); the specific surface area of AC* increased by 29.43%, while the surface area of CNT* was slightly lower than before the modification, reduced by 9.94%. However, the micropore volume of AC* and CNT* increased by 28.12% and 48.28% respectively.

Electrochemical performance of the electrode

The cyclic voltammetry test of different AC*/CNT* composite electrodes used a three-electrode system. The graph of cyclic voltammograms for different electrodes at 1 V voltage, 2 mV/s scan speed, and 1 mol/L KCl electrolyte is shown in Figure S2(a) (Supporting Information, available online). The symmetry of each curve is good and approximately rectangular, indicating that each electrode has good cycle stability and can perform multiple cycle adsorption–desorption processes. According to Equation (1), the specific capacitance was 130.48 F/g, 81.62 F/g, 78.01 F/g, 76.13 F/g and 68.30 F/g as the CNT* added in the AC* was 10%, 20%, 30%, 40% and 50% respectively, that is, the specific capacitance of the electrodes fabricated by AC*, CNT* and PVDF according to the mass ratio of 7.2:0.8:2 was the best.

The electrochemical impedance spectroscopy Nyquist diagram of different AC*/CNT* composite electrodes is shown in Figure S2(b). The arc diameter decreased with the increase of the content of CNT*, which indicating that the resistance to the charge transfer process became weaker and the addition of CNT* could increase the electrical conductivity of the electrode coating significantly, that is, the electrode impedance of the electrodes fabricated by AC*, CNT* and PVDF according to the mass ratio of 7.2:0.8:2 was the best.

Study of electrode regeneration

The electrode regeneration of the composite electrode was studied (see Figure S3 in the Supporting Information, available online), and the adsorption and desorption cycles of the AC*/CNT* composite electrode were very stable. After a period of continuous adsorption–desorption, the electrode's electrosorption performance hardly decreased, and the

surface remained intact without falling off. The desorption rate of the initial desorption was up to 97.73% after reaching electric adsorption equilibrium. Although the desorption effect slowly deteriorated during the subsequent desalination process, the desorption rate still exceeded 90%.

Analysis of adsorption kinetics and electromigration

In order to understand the ion transfer process in the coating in detail, the adsorption kinetics under different operating voltages was investigated. The adsorption process was fitted by the pseudo-first-order and pseudo-second-order kinetics equations. Sodium chloride solution of 50 mL with concentration of 100 mg/L (conductivity of 220 μS/cm) was prepared, and the operating voltage was controlled at 0.8 V, 1.0 V, 1.2 V and 1.4 V, respectively. As shown in Figure 1(a) and 1(b), the pseudo-first-order and pseudo-second-order kinetics equations were used to fit the operating data of the AC*/CNT* composite electrode at the different operating voltages. The detailed parameters of the fitting are listed in Table 1.

Under the condition of initial water inflow of 5 mL/min and electrode spacing of 3 mm, 200 mL sodium chloride solutions with initial water concentrations of 50 mg/L, 100 mg/L, 150 mg/L, 200 mg/L and 250 mg/L were prepared respectively, the operating voltages applied to the two electrode plates being 0.8 V, 1.0 V, 1.2 V, and 1.4 V, respectively. The CDI test was carried out to investigate the adsorption capacity of the AC*/CNT* composite electrode and the adsorption type of CDI adsorption process under different concentrations and different voltages. As shown in Figure 1(c) and 1(d), there are two isotherm adsorption models, Langmuir and Freundlich, respectively. The curves were obtained by fitting the AC*/CNT* composite electrode to the operating data of different operating voltages and different initial influent concentrations, and detailed parameters are listed in Table 2.

As shown in Table 1, two kinetics equations could fit the data obtained in the experiment perfectly under the four different working voltage conditions, and the fitting regression constant R^2 was greater than 0.99, moreover, the adsorption rates of the two reaction kinetics increased with the increase of the working voltage. However, at the

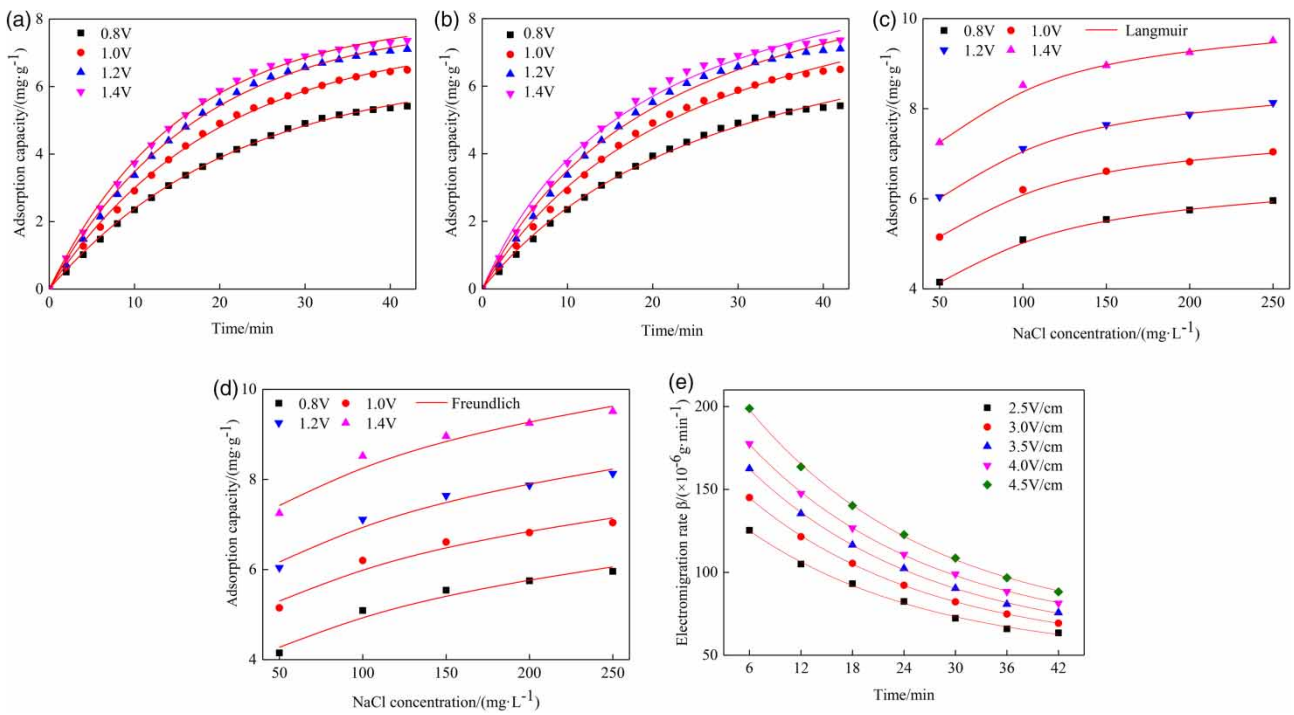

Figure 1 | (a), (b) Pseudo-first-order kinetics fitting and Pseudo-second-order kinetics fitting at different operating voltages; (c), (d) Langmuir adsorption isotherm fitting and Freundlich adsorption isotherm fitting at different operating voltages; (e) electromigration fitting at different potential gradients.

Table 1 | Correlation parameters of two kinds of kinetics fitting at different operating voltages

		Pseudo-first-order kinetics adsorption equation			Pseudo-second-order kinetics adsorption equation		
Voltage (V)	Experimental adsorption capacity (mg/g)	q_e (mg/g)	k_1($\times10^{-2}$ min^{-1})	R^2	q_e(mg/g)	k_1($\times10^{-2}$ min^{-1})	R^2
0.8	5.42	6.48	4.58	0.9989	9.61	0.348	0.9976
1.0	6.49	7.48	5.12	0.9982	10.85	0.357	0.9960
1.2	7.11	7.96	5.74	0.9979	11.28	0.400	0.9949
1.4	7.36	8.03	6.41	0.9985	11.09	0.478	0.9948

same working voltage, the fitting regression constant R^2 of the pseudo-first-order kinetics was always higher than the pseudo-second-order kinetics, closer to 1. The theoretical saturated adsorption capacity of the pseudo-first-order kinetics was not only increased with the increase of voltage, but was also closer to the experimental equilibrium adsorption capacity, yet the pseudo-second-order kinetics did not increase with the increase of voltage (the theoretical saturated adsorption capacity at 1.2 V was greater than the theoretical saturated adsorption at 1.4 V), and the trend of variation was contrary to the trend of saturated adsorption obtained in the actual experiments. Therefore, the Lagergren equation in the pseudo-first-order kinetics can more accurately and perfectly reflect the adsorption rate of the AC*/CNT* composite electrode during CDI operation than in the pseudo-second-order kinetics. In addition, as can be seen from Figure 1(a), the electrode had the largest adsorption capacity when the operating voltage was 1.4 V. However, there were a large number of micro-bubbles continuously generated on the surface of the electrode, indicating that the electrode coating had exceeded the theoretical decomposition voltage of water, the electrolysis reaction of water was occurring and a Faraday current was being produced; the occurrence of the Faraday reaction would seriously affect the cycle number of the electrode and reduce its service life. Therefore, 1.2 V was chosen as the best working voltage and the specific adsorption amount was 7.11 mg/g.

As shown in Table 2, the adsorption equilibrium constant K_L increased continuously when the working voltage increased from 0.8 V to 1.0 V, 1.2 V and 1.4 V, illustrating that the higher the working voltage, the stronger the adsorption capacity of the AC*/CNT* composite electrode coating for ions in the salt water, and the larger the maximum adsorption capacity q_m. The values of n in the table are all above 4, that is, $1/n < 0.3$, showing that the adsorption process of capacitive deionization was of an easily adsorbable type. The R^2 of the Langmuir model in the range of the selected working voltage and the initial concentration of the sodium chloride solution exceeded 0.99 and was larger than the R^2 of the Freundlich model. The results show that the Langmuir model can better fit and describe the adsorption mechanism of the AC*/CNT* composite electrode during CDI operation, that is, the adsorption process in CDI operation is mainly carried out by single ion layer adsorption.

Under the condition of initial water inflow of 5 mL/min and electrode spacing of 3 mm, 50 mL of sodium chloride solution with 100 mg/L of initial water concentration was

Table 2 | Correlation parameters of two adsorption isotherm fittings at different operating voltages

		Langmuir			Freundlich		
Voltage (V)	Experimental adsorption capacity (mg/g)	q_m(mg/g)	K_L($\times10^{-2}$)	R^2	K_F	n	R^2
0.8	5.96	6.65	3.29	0.9991	1.83	4.62	0.9737
1.0	7.04	7.71	4.04	0.9987	2.70	5.69	0.9655
1.2	8.13	8.83	4.26	0.9974	3.59	5.58	0.9779
1.4	9.51	10.24	4.85	0.9980	3.94	6.19	0.9680

Table 3 | Correlation parameters of electro-migration at different potential gradients ($\times 10^{-6}$ g/min)

Potential gradient (V/cm)	A	B	C	R^2	Corresponding equation
2.5	48.19	101.68	−0.047	0.9983	$Y = 48.19 + 101.68\exp(-0.047t)$
3.0	52.13	122.80	−0.047	0.9998	$Y = 52.13 + 122.80\exp(-0.047t)$
3.5	55.32	141.51	−0.047	0.9994	$Y = 55.32 + 141.51\exp(-0.047t)$
4.0	59.83	155.81	−0.047	0.9995	$Y = 59.83 + 155.81\exp(-0.047t)$
4.5	63.89	177.48	−0.047	0.9991	$Y = 63.89 + 177.48\exp(-0.047t)$

prepared, and the working voltages applied to the two electrode plates were 0.8 V, 1.0 V, 1.2 V, 1.4 V, respectively. Electromigration fitting at different potential gradients is shown in Figure 1(e), and the relevant parameters and formulas after fitting are listed in Table 3.

As shown in Figure 1(e) and Table 3, the ionic mobility increased with the increase of the potential gradient, showing that the ionic mobility is proportional to the working voltage; at the same time, the electromigration rate of ions increased with the prolongation of CDI desalination time, but the increase rate was gradually reduced, indicating that when the potential gradient is large, the charged particles can quickly move into the coating material of the electrode surface in a short time. Table 3 shows that the trend of electromobility of charged particles in saline water can be well fitted by exponential equations.

CONCLUSIONS

An AC*/CNT* composite electrode was fabricated through mixing acid modification. After modification, the specific surface area and pore volume of AC* increased significantly and the specific surface area of CNT* decreased slightly, but the pore diameter increased and the dispersibility was effectively improved. The specific capacitance of electrodes fabricated by AC*, CNT* and PVDC according to the mass ratio of 7.2:0.8:2 was the best, reaching 130.48 F/g. The AC*/CNT* composite electrode also presented was excellent regenerability and stability. Study of the desalination mechanism of the AC*/CNT* composite electrode shows that the R^2 value of the pseudo-first-order kinetics model is larger than the R^2 of the pseudo-second-order kinetics under different working voltage conditions, and the theoretical saturated adsorption amount of the former is closer to the experimental saturated adsorption amount; the Langmuir model can better fit and describe the adsorption mechanism of the AC*/CNT* composite electrode in the CDI desalination process; the electromigration of the CDI process of the AC*/CNT* composite electrode is found to be proportional to the working voltage, moreover, the trend of ion mobility with migration time can be well fitted by exponential equations. These results demonstrated that the AC*/CNT* composite electrode can be used as a promising electrode material for CDI technology.

ACKNOWLEDGEMENTS

This study was supported by the National Natural Science Foundation (51574185) and Provincial Key Laboratory Project, Wuhan, China.

REFERENCES

Bian, Y. H., Liang, P., Yang, X. F., Jiang, Y., Zhang, C. Y. & Huang, X. 2016 Using activated carbon fiber separators to enhance the desalination rate of membrane capacitive deionization. *Desalination* **381**, 95–99.

Dursun, D., Ozkul, S., Yuksel, R. & Unalan, H. E. 2017 Enhancing capacitive deionization technology as an effective method for water treatment using commercially available graphene. *Water Science and Technology* **75** (3), 643–649.

Fang, C. H., Liu, P. I., Chung, L. C., Shao, H., Ho, C. H., Chen, R. S., Fan, H. T., Liang, T. M., Chang, M. C. & Horng, R. Y. 2016 A flexible and hydrophobic polyurethane elastomer used as binder for the activated carbon electrode in capacitive deionization. *Desalination* **399**, 34–39.

Hou, C. H., Huang, C. Y. & Hu, C. Y. 2013 Application of capacitive deionization technology to the removal of sodium

chloride from aqueous solutions. *International Journal of Environmental Science & Technology* **10** (4), 753–760.

Hou, C. H., Liu, N. L., Hsu, H. L. & Den, W. 2014 Development of multi-walled carbon nanotube/poly(vinyl alcohol) composite as electrode for capacitive deionization. *Separation and Purification Technology* **130**, 7–14.

Huang, W., Zhang, Y. M., Bao, S. X., Cruz, R. & Song, S. X. 2014 Desalination by capacitive deionization process using nitric acid-modified activated carbon as the electrodes. *Desalination* **340**, 67–72.

Iftekhar, S., Farooq, M. U., Sillanpää, M., Asif, M. B. & Habib, R. 2016 Removal of Ni(II) using multi-walled carbon nanotubes electrodes: relation between operating parameters and capacitive deionization performance. *Arabian Journal for Science & Engineering* **42**, 235–240.

Jo, H., Kim, K. H., Jung, M. J., Park, J. H. & Lee, Y. S. 2017 Fluorination effect of activated carbons on performance of asymmetric capacitive deionization. *Applied Surface Science* **409**, 117–123.

Kang, J., Kim, T., Shin, H., Lee, J., Ha, J. I. & Yoon, J. 2016 Direct energy recovery system for membrane capacitive deionization. *Desalination* **398**, 144–150.

Kohli, D. K., Singh, R., Singh, M. K., Singh, A., Khardekar, R. K., Sankar, P. R., Tiwari, P. & Gupta, P. K. 2012 Study of carbon aerogel-activated carbon composite electrodes for capacitive deionization application. *Desalination and Water Treatment* **49** (1–3), 130–135.

Kumar, R., Gupta, S. S., Katiyar, S., Raman, V. K., Varigala, S. K., Pradeep, T. & Sharma, A. 2016 Carbon aerogels through organo-inorganic co-assembly and their application in water desalination by capacitive deionization. *Carbon* **99**, 375–383.

Li, H. B., Ma, Y. L. & Niu, R. 2016 Improved capacitive deionization performance by coupling TiO_2 nanoparticles with carbon nanotubes. *Separation and Purification Technology* **171**, 93–100.

Liu, P. I., Chung, L. C., Ho, C. H., Shao, H., Liang, T. M., Chang, M. C., Ma, C. C. M. & Horng, R. Y. 2016 Comparative insight into the capacitive deionization behavior of the activated carbon electrodes by two electrochemical techniques. *Desalination* **379**, 34–41.

Mossad, M. & Zou, L. 2012 Study of fouling and scaling in capacitive deionisation by using dissolved organic and inorganic salts. *Journal of Hazardous Materials* **244-245**, 387–393.

Orha, C., Pode, R., Manea, F., Lazau, C. & Bandas, C. 2017 Titanium dioxide-modified activated carbon for advanced drinking water treatment. *Process Safety and Environmental Protection* **108**, 26–33.

Porada, S., Zhao, R., van der Wal, A., Presser, V. & Biesheuvel, P. M. 2013 Review on the science and technology of water desalination by capacitive deionization. *Progress in Materials Science* **58** (8), 1388–1442.

Santoro, C., Abad, F. B., Serov, A., Kodali, M., Howe, K. J., Soavi, F. & Atanassov, P. 2017 Supercapacitive microbial desalination cells: new class of power generating devices for reduction of salinity content. *Applied Energy* **208**, 25–36.

Tuan, T. N., Chung, S., Lee, J. K. & Lee, J. 2015 Improvement of water softening efficiency in capacitive deionization by ultra purification process of reduced graphene oxide. *Current Applied Physics* **15** (11), 1397–1401.

Wang, L., Zhou, Y., Wang, J. & Hu, N. 2015 Approaching capacitive deionization (CDI) on desalination of water and wastewater – new progress and its potential. *Advanced Materials Research* **1088** (3), 557–561.

Wang, L., Lei, L., Zhou, Y. & Fu, J. T. 2017 Fabrication of titanium carburizing electrodes for capacitive deionization. *Water Science and Technology* **76** (4), 754–760.

Wu, T. T., Wang, G., Dong, Q., Qian, B. Q., Meng, Y. L. & Qiu, J. S. 2015 Asymmetric capacitive deionization utilizing nitric acid treated activated carbon fiber as the cathode. *Electrochimica Acta* **176**, 426–433.

Xu, X. T., Pan, L. K., Liu, Y., Lu, T. & Sun, Z. 2015 Enhanced capacitive deionization performance of graphene by nitrogen doping. *Journal of Colloid and Interface Science* **445**, 143–150.

First received 28 December 2018; accepted in revised form 18 May 2019. Available online 3 June 2019